AIMS Mathematics, 11(1): 1616–1636.
DOI: 10.3934/math.2026067
Received: 14 September 2025
Revised: 21 November 2025
Accepted: 25 November 2025
Published: 19 January 2026

http://www.aimspress.com/journal/Math

Research article

Chaos modeling of a symmetrical Jerk system via analog circuit design and radial basis function neural network

Aceng Sambas[1,*], Hatem E. Semary[2], Abdullah Gokyildirim[3], Sadam Hussain[4], Rameshbabu Ramar[5], Sulaiman M. Ibrahim[6,*], A. S. Al-Moisheer[2] and Rabiu Bashir Yunus[7]

[1] Department of Mechanical Engineering, Universitas Muhammadiyah Tasikmalaya, Tasikmalaya, 46196, Indonesia
[2] Department of Mathematics and Statistics, College of Science, Imam Mohammad Ibn Saud Islamic University (IMSIU), Riyadh 11432, Saudi Arabia
[3] Department of Electrical and Electronics Engineering, Faculty of Engineering and Natural Sciences, Bandirma Onyedi Eylul University, Bandirma 10200, Balikesir, Turkey
[4] School of Science, Harbin Institute of Technology, Shenzhen 518055, China
[5] Department of Electronics and Communication Engineering, V.S.B. Engineering College, Karur, 639111, Tamil Nadu, India
[6] College of Applied and Health Sciences, A'Sharqiyah University, Post Box No. 42, Post Code No. 400 Ibra, Sultanate of Oman
[7] Department of Mathematics, Faculty of Computing and Mathematical Sciences, Aliko Dangote University of Science and Technology Wudil, Kano, 713101, Nigeria

* **Correspondence:** Email: acengs@umtas.ac.id, sulaimancga@gmail.com.

Abstract: In this paper, we investigated the chaotic behavior of a Jerk system proposed by Sambas et al. (2024), which features symmetrical attractors arising from the interplay of sinusoidal, hyperbolic, and absolute nonlinearities. The system's complex dynamics were analyzed using established numerical methods such as phase portraits, stability analysis, bifurcation diagrams, and Lyapunov exponents. Furthermore, through amplitude modulation, we showed that the control parameter δ can enhance or attenuate signal amplitudes without disrupting the system's stability or chaotic nature. The theoretical findings were further validated through Multisim circuit simulations, with experimental attractors closely matching the numerical results. In addition, a Radial Basis Function Neural Network (RBFNN) was implemented to approximate the chaotic trajectories of the system. The model was trained using simulated data and optimized via the least squares method. Network performance was

evaluated using Root Mean Square Error (RMSE) and relative error. The results showed that the RBFNN accurately predicts the system's state variables, achieving MSE values on the order of 10^{-10}–10^{-9} and relative error below 1.1×10^{-8}.

Keywords: chaotic system; Jerk circuit; circuit design; RBFNN
Mathematics Subject Classification: 34C28, 37C10, 37D45, 94C05, 68T07

1. Introduction

Chaotic behavior arises from the nonlinear interactions among system components [1–3]. Unlike linear systems, where input-output relationships follow simple mathematical rules, nonlinear systems exhibit complex and often unpredictable behavior [4]. Chaotic systems within electronic circuits are those that demonstrate chaotic traits, marked by their sensitivity to initial conditions, non-repeating long-term patterns, and deterministic nature [5]. These systems typically employ nonlinear electronic elements like diodes, transistors, operational amplifiers, and capacitors for their implementation [6].

One of the most famous examples of a chaotic electronic circuit is Jerk circuit, a dynamical system characterized by the presence of jerk, which is the rate of change of acceleration with respect to time [7]. In chaotic jerk systems, the evolution of the system's state variables exhibits chaotic behavior. The equations describing a chaotic jerk system typically involve nonlinearity and may include terms representing damping, external forcing, and nonlinear interactions among state variables [8]. The inclusion of jerk in the system dynamics introduces additional complexity compared to systems described solely by position, velocity, and acceleration [9,10].

Numerous publications have focused on the research topic of Jerk circuits for generating chaotic attractors. Srisuchinwong & Treetanakorn [11] introduced a novel current-tunable chaotic jerk circuit employing a single unity-gain amplifier, exhibiting a homoclinic orbit. Kengne et al. [12] proposed a self-driven RC chaotic jerk circuit featuring smoothly adjustable nonlinearity, resulting in symmetric double scroll chaos. Chiu et al. [13] developed a jerk circuit implementation using a hybrid analog–digital system, applied in digital circuits such as microcontrollers and DAC/ADC boards. Chansangiam [14] explored the chaotic behavior of a modified jerk circuit incorporating Chua's diode, with the system exhibiting a symmetric piecewise linear voltage-current characteristic. Ding and Feng [15] presented a novel chaotic system generating multi-scroll attractors based on a Jerk circuit utilizing a special form of a sine function. Li et al. [16] investigated an equilibrium-free piecewise linear jerk system employing a signum operation, resulting in hidden attractors. Joshi and Ranjan [17] proposed a simple jerk system with sine hyperbolic nonlinearity, yielding hidden attractors, and designed an electrical circuit implementation using a single amplifier and few passive elements. Mboupda Pone [18] examined an autonomous jerk circuit with quintic nonlinearity, leading to period-doubling route to chaos, bistability, and antimonotonicity. Ainamon et al. [19] designed an autonomous three-dimensional Helmholtz-type oscillator generating Hopf bifurcation, bistable period-2 limit cycles, and coexisting attractors. Ahmad & Srisuchinwong [20] introduced 3D dissipative chaotic jerk flows with different families of self-excited and hidden attractors, including systems with single all-zero-eigenvalue non-hyperbolic equilibrium or two symmetrical hyperbolic equilibria. Sambas et al. [21] designed a novel jerk chaotic oscillator with symmetric attractors, modeled it using a neural network, and applied it to a robust chaos-based image encryption algorithm. Arshad et al. [22] studied the

general jerk equation with a scaled sine map, approximating it in terms of a polynomial using Taylor series expansion to exhibit chaotic behavior. Xu et al. [23] proposed an asymmetric memristive diode-bridge with asymmetric volt-ampere characteristic, resulting in asymmetric coexisting bifurcations and multi-stability phenomena.

Controlling nonlinear and chaotic systems presents significant challenges, primarily due to their sensitive dependence on initial conditions and strong nonlinearity [24]. These systems often exhibit unpredictable behavior that changes drastically over time. Even small variations in the initial state can cause the system to diverge rapidly. This sensitivity makes precise and reliable control extremely difficult to achieve [25]. Traditional control strategies, such as PID or linear state feedback controllers, are often inadequate for maintaining desired performance in such environments. They assume predictable system responses, which is rarely the case in chaotic dynamics [26]. Consequently, researchers have explored more adaptive and flexible control frameworks. Among these, intelligent control techniques have emerged as powerful alternatives for handling chaos.

Over the past decades, RBFNN have gained considerable attention due to their powerful approximation capabilities and simplicity of architecture. Researchers have successfully applied RBFNN in various domains such as direct torque control for PMSM [27], detection of Parkinson's disease [28], predicting a photovoltaic fed electric vehicle charging station [29], controlling a 3-DOF helicopter system [30], controlling a doubly fed induction generator [31], controlling a lower limb exoskeleton robot [32], predicting of suspender frequency and tension on arch bridge [33], and controlling coaxial hybrid aerial–underwater vehicles [34]. Most researchers looking at chaotic jerk systems have focused on system modeling, bifurcation analysis, and analog circuit implementation. However, limited attention has been given to intelligent modeling approaches that can learn and predict chaotic trajectories accurately. To date, the integration of RBFNN for precise approximation and control of chaotic jerk dynamics remains underexplored.

The main contribution and novelty of this work is as follows:

a. We show that the control parameter δ can enhance or attenuate signal amplitudes without disrupting the system's stability or chaotic nature
b. We implement a complete analog circuit validation using Multisim and experimental verification with high accuracy.
c. We introduce the RBFNN framework to model and predict the chaotic system's behavior, achieving high precision with MSE values on the order of 10^{-10}-10^{-9} and relative error below 1.1×10^{-8}.

The structure of the paper is outlined as follows: In Section 2, we focus on the modeling process of the jerk circuit and examine the stability of the equilibrium points. In Section 3, we note that the control parameter δ can amplify or diminish the system's signals without compromising stability or chaotic behavior. The experimental investigation of the oscillator is conducted in Section 4. Laboratory experimental measurements demonstrate a high degree of agreement with the theoretical analyses. In Section 5, we introduce the application of RBFNN to model and approximate the chaotic trajectories of the proposed jerk system, validating the system's behavior through machine learning techniques. Finally, in Section 6, we present concluding remarks, emphasizing the accuracy of RBFNN in capturing the system dynamics and suggesting its potential for future intelligent control applications.

2. System description

In this study, we employ the Jerk circuit initially introduced by Sambas et al. in 2024 [21], which is a 3D autonomous nonlinear system. The system is governed by the following set of ordinary differential equations:

$$\begin{cases} \dot{x} = y \\ \dot{y} = az \\ \dot{z} = x - by - cz - |x| \sinh(x) \end{cases} \tag{1}$$

where

- (x, y, z) are the state variables representing position, velocity, and jerk, respectively.
- $a > 0$, $b > 0$, and $c > 0$ are system parameters controlling damping, feedback strength, and nonlinear gain.
- $\sinh(x)$ provides **unbounded hyperbolic growth** and introduces stronger symmetry.
- $|x|$ introduces **piecewise linear behavior** enhancing slope-based nonlinearity.

We assume that X denotes the state (x, y, z) and $a = 0.4, b = 0.72, c = 0.48$ are positive constants.

The jerk system (1) exhibits rotation symmetry with respect to the z-axis. This means that if the system is subjected to a rotation in the (x, y) plane by any angle θ does not change the structure of the vector field. Let a rotation in the (x, y) plane be defined as:

$$\begin{pmatrix} x^* \\ y^* \end{pmatrix} = \begin{pmatrix} \cos\theta & -\sin\theta \\ \sin\theta & \cos\theta \end{pmatrix} \begin{pmatrix} x \\ y \end{pmatrix}, \quad z^* = z\,. \tag{2}$$

Applying this transformation to system (1), the nonlinear terms sinh(x) and |x| depend only on the magnitude of |x|, and not on their orientation in the plane. Therefore, the transformed system satisfies:

$$\dot{x}^* = \dot{x}\cos\theta - \dot{y}\sin\theta, \;\; \dot{y}^* = \dot{x}\sin\theta + \dot{y}\cos\theta, \tag{3}$$

which shows that the vector field rotates consistently with the variables. Therefore, system (1) is invariant under rotation in the (x, y) plane, confirming rotational symmetry about the z-axis.

In our other study [21], we encountered difficulties in experimentally validating the circuit in the laboratory, as the oscilloscope failed to display the expected theoretical results. However, after modifying the system parameters to $a = 4, b = 0.85$ and $c = 0.55$, we successfully captured the phase portraits on the oscilloscope. Remarkably, these experimental results closely matched the theoretical phase portraits obtained through MATLAB simulations.

The Lyapunov exponents for the jerk system (1) for these parameter values and initial values were computed using MATLAB as $L_1 = 0.0976, L_2 = 0$, and $L_3 = -0.6476$. Thus, the jerk system (1) has dissipative motion with a chaotic attractor. The chaotic system of the jerk system (1) has the Kaplan dimension given by

$$D_K = 2 + \frac{L_1 + L_2}{|L_3|} = 2.1507\,. \tag{4}$$

Figure 1 shows the MATLAB signal plots of the jerk system (1) for the parameter values taken as $a = 4, b = 0.85, c = 0.55$ and the initial state $x(0) = 0.1, y(0) = 0.1$, and $z(0) = 0.2$.

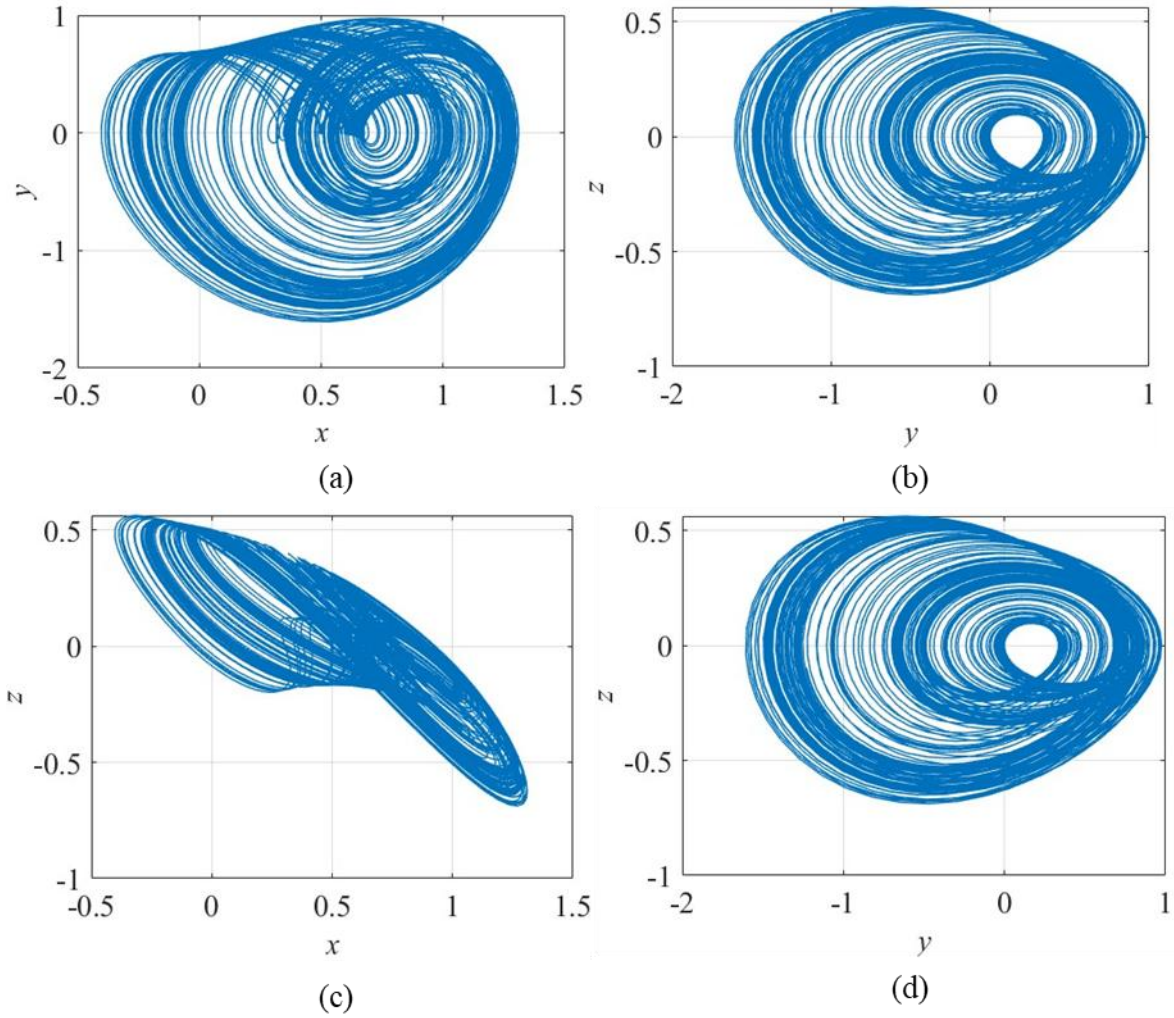

Figure 1. Chaotic attractors of the proposed system (1): (a) $x-y$ plane, (b) $y-z$ plane, (c), $x-z$ plane and (d) 3D model for $a=4, b=0.85, c=0.55$ with the initial state $x(0)=0.1, y(0)=0.1$, and $z(0)=0.2$.

3. Amplitude control

In this section, the amplitude of the chaotic signals is amplified and attenuated by rescaling the signals with a constant parameter. If we take $x \to \delta x$, $y \to \delta y$, and $z \to \delta z$ in the system (1), then system (1) becomes to complete amplitude controllable system, where δ is the total amplitude controller. The complete amplitude controllable system is given in Eq (5).

$$\begin{aligned} \dot{x} &= y \\ \dot{y} &= az \\ \dot{z} &= x - by - cz - |x|\sinh(\delta x) \end{aligned} \quad . \tag{5}$$

The control parameter δ amplifies or attenuates all the three signals x, y, and z without affecting the chaotic dynamics of the system (5). The modulation parameter δ in the amplitude-controlled formulation serves as a global scaling factor that uniformly adjusts the magnitude of all state variables in the Jerk system. This parameter plays an important engineering role because many practical chaotic circuits require control over a signal amplitude without altering the intrinsic nonlinear dynamics. In

real implementations, such as analog chaotic oscillators, communication circuits, and signal-conditioning modules, amplitude levels must be tuned to prevent component saturation, ensure compatibility with ADC/DAC converters, or match the voltage range of downstream circuitry. This property makes δ especially valuable when the chaotic oscillator is integrated into larger engineering systems where amplitude tuning is required but dynamical integrity must remain intact. Thus, the inclusion of the modulation parameter δ provides a practical degree of control that enhances the utility of the proposed chaotic Jerk system for real-world electronic and signal-processing applications.

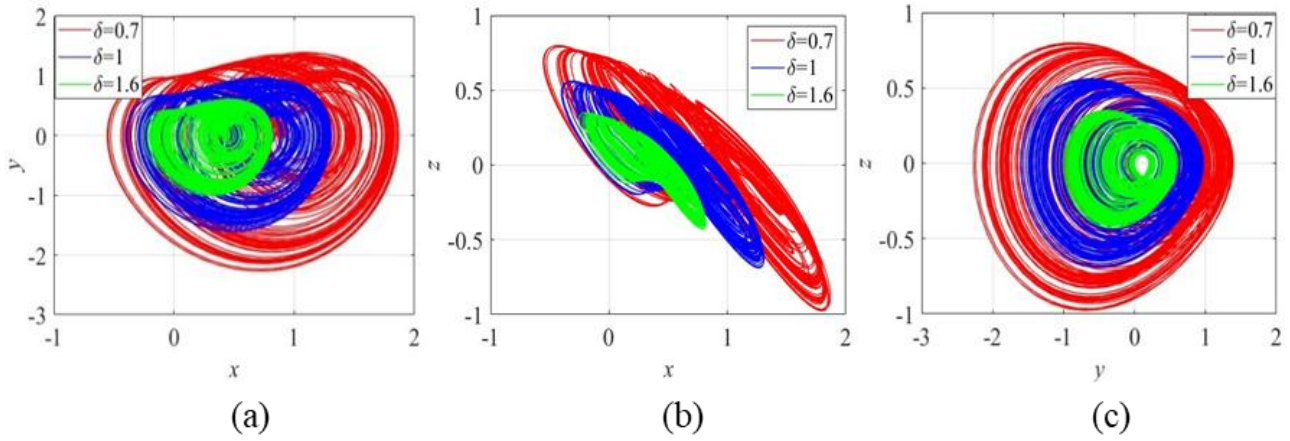

Figure 2. The complete amplitude-controlled attractors with $\delta = 1$ (Blue), $\delta = 0.7$ (Red) and $\delta = 1.6$ (Green) (a) $x - y$ plane, (b) $x - z$ plane, (c) $y - z$ plane, and (d) 3D model.

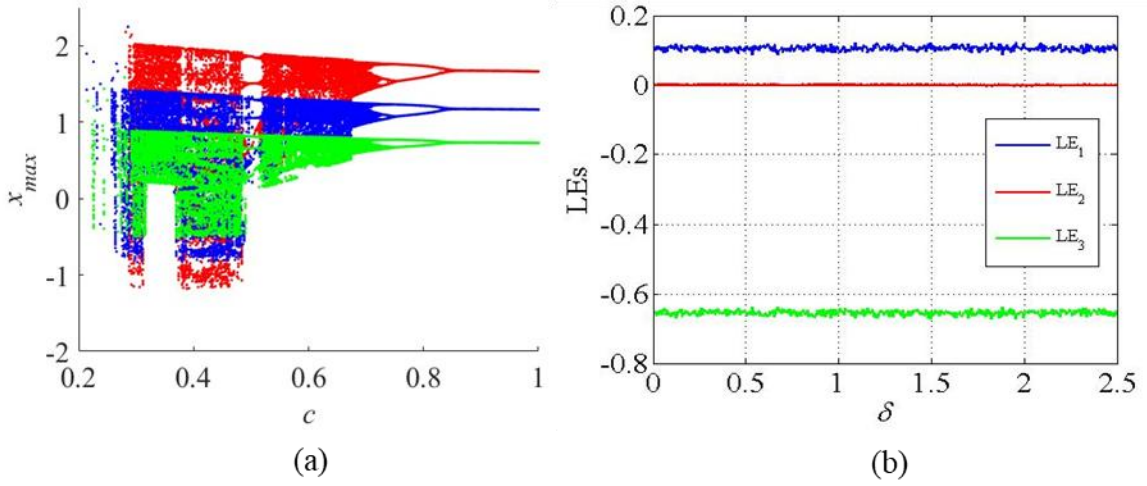

Figure 3. (a) Bifurcation diagram of system (5) when $\delta = 1$ (Blue), $\delta = 0.7$ (Red), and $\delta = 1.6$ (Green). (b) Lyapunov exponent spectrum of the system (5) under the control parameter δ.

Figure 2 indicates the attractors of the amplitude controllable system with $\delta = 1$ (Blue), $\delta = 0.7$ (Red) and $\delta = 1.6$ (Green). The control parameter δ amplifies the signal when $\delta < 1$ and attenuates

when $\delta > 1$. Figure 3a shows the bifurcation diagram of the system (1) under parameter c with $\delta = 1$ (Blue), $\delta = 0.7$ (Red), and $\delta = 1.6$ (Green). This indicates that control parameter δ controls the amplitude of the system without modifying its states. Figure 3b shows the Lyapunov exponent spectrum of system (5) under control parameter δ. This indicates that Lyapunov exponent values of the system (5) are not modified by the control parameter δ. Thus, we can conclude that the control parameter δ amplifies or attenuates the signals of the system (5) without affecting its stability and the chaotic behaviors.

4. Electronic circuit implementation

Developments have also demonstrated that nonlinear functions commonly used in chaotic systems, such as the hyperbolic term sinh*(δx)* in our model, can be efficiently approximated in the digital domain, enabling high-speed, low-power, and numerically stable realizations. For instance, [35] and [36] show that trigonometric and hyperbolic nonlinearities can be implemented using polynomial or lookup-table based approximations with excellent accuracy for real-time chaotic applications. Although analog circuits based on operational amplifiers are widely used for experimental verification, they generally require relatively high voltage bias and provide limited frequency response compared to digital implementations or CMOS-based realizations. In this regard, CMOS integrated designs, such as those presented in [37] and [38], demonstrate that chaotic oscillators can be implemented with much lower power consumption, wider bandwidth, and significantly reduced chip area. These developments indicate that the proposed jerk system also holds strong potential for future realization using digital or CMOS technology.

In this section, the implementation of the electronic circuit for the novel oscillator. To achieve this, the resistance and capacitance values for the circuit are determined. Following this, the application and simulation results are compared. The electronic circuit implementation of the novel jerk oscillator in the OrCAD-PSpice simulation program is shown in Figure 4. The control parameter and the initial conditions of the system are chosen as $a = 4$, $b = 0.85$, $c = 0.55$, and $x(0) = 0.1$, $y(0) = 0.1$, and $z(0) = 0.2$, respectively.

The designed circuit that emulates Jerk system (1) consists of three capacitors, seventeen resistors, four diodes (1N4148), a multiplexer (AD633JN), and eight operational amplifiers (TL081CN). The nonlinear part of the 3D Jerk system (1) includes a diode pair (D_1 and D_2) used to describe the sinh(x) function. The current, through each of the antiparallel diodes, is given by [39]:

$$I = 2I_S \sinh\left(\frac{v}{nV_T}\right) \tag{6}$$

where n represents the diode ideality factor, I_S is the reverse bias saturation current, v represents the voltage across the diodes, and V_T denotes the thermal voltage. The equation (6) is derived by applying Kirchhoff's current law and utilizing the well-known Shockley diode equation for the two antiparallel diodes. D_1 and D_2 are used as 1N4148 diodes, with the following specifications: n=1.9, I_S = 26.2 nA, and V_T = 26mV [40]. Considering Figure 4, the dimensionless equations of the Jerk system (1) are described as follows:

$$
\begin{aligned}
RC_1 \frac{dv_x}{dt} &= \frac{Rv_y}{R_1}, \\
RC_2 \frac{dv_y}{dt} &= \frac{Rv_z}{R_2}, \\
RC_3 \frac{dv_z}{dt} &= \frac{Rv_x}{R_3} - \frac{Rv_y}{R_4} - \frac{Rv_z}{R_5} - \frac{2RI_s \sinh(v_x/nV_T)|v_x|}{10R_6},
\end{aligned} \tag{7}
$$

The time scale factor RC is calculated as 0.133ms. DC power supply values are selected as V_P = -V_N = 15V. Figure 5 shows the voltages on the X, Y, and Z terminals plotted against each other.

To enhance reproducibility, we provide a more detailed description of the parameters and component settings used in the Multisim implementation. All simulations were conducted in Multisim 14.2 using the default SPICE models provided in the component library. The Multisim simulation was configured with a maximum timestep of 10 μs, Gear integration mode, and 50 ms total simulation time, as these settings produced stable and accurate reproduction of the chaotic attractors. The electronic circuit can be seen in Table 1.

Table 1. Summary of electronic components used in the circuit implementation.

Component type	Quantity	Specification/Value
Operational amplifiers	8	TL081CN
Analog multiplier	1	AD633JN
Resistors	17	R1 = R6 = 400 kΩ; R2 = 100 kΩ; R3 = 40 kΩ; R4 = 471 kΩ; R5 = 727 kΩ; R7–R17 = 10 kΩ
Capacitors	3	0.33 nF
Diodes	4	1N4148 (two antiparallel pairs)
DC power supply	1	± 15 V

The FFT results shown in Figure 6 provide additional confirmation of the chaotic nature of the proposed jerk system. The spectra exhibit a broadband and irregular distribution of frequency components without any dominant peaks, which is a key signature of chaotic oscillations. This frequency-domain behavior complements the time-domain phase portraits and reinforces that the circuit implementation reproduces the system's aperiodic dynamics.

The discrete component electronic circuit of the novel system is constructed on a board for comparison with the PSpice simulation results. As can be observed from the oscilloscope images shown in Figure 7, the experimental results obtained from the circuit established are quite similar to the simulation results in Figure 1. Finally, Figure 8 illustrates the experimental setup of the novel system.

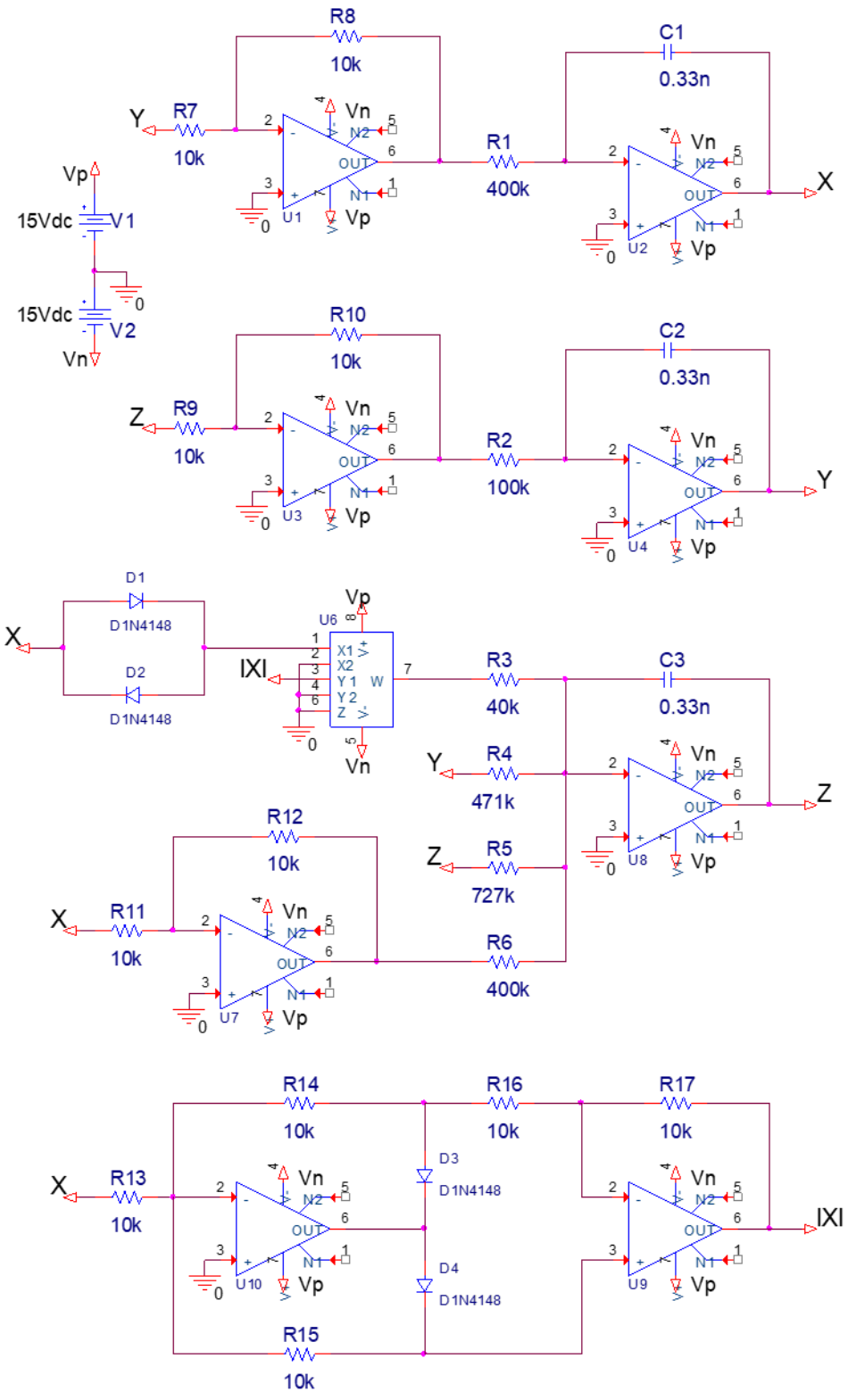

Figure 4. Electronic circuit schematic of the novel system.

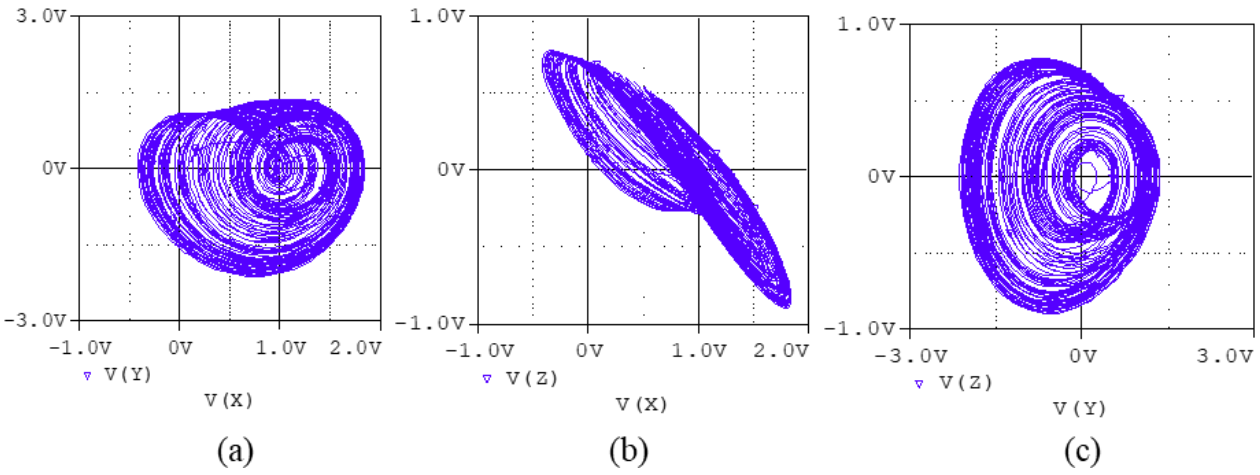

Figure 5. Phase portraits of the novel system in PSpice simulation for t=50ms and maximum step size=10μs: (a) v_x-v_y, (b) v_x-v_z, and (c) v_y-v_z.

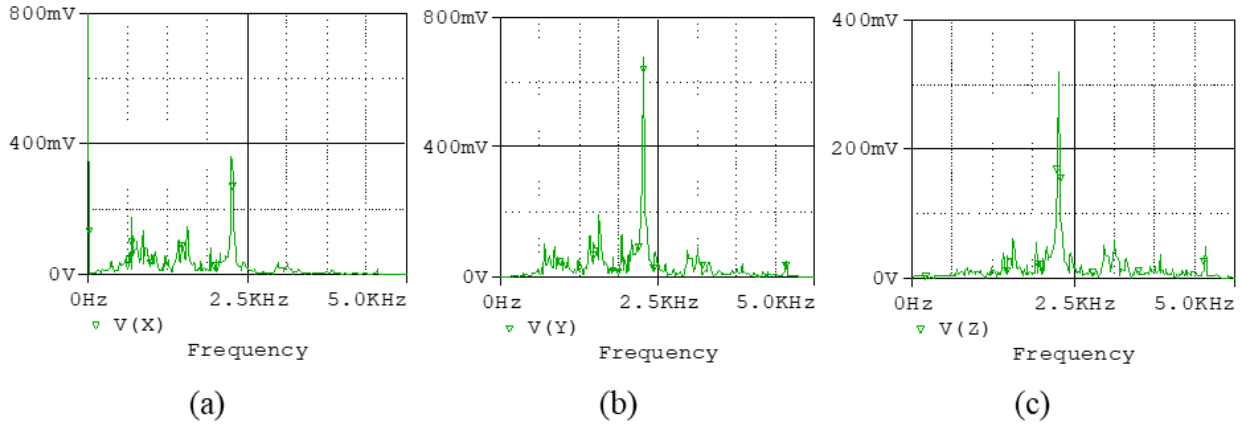

Figure 6. FFT analyses results in the PSpice program: (a) FFT spectrum of the V(x) signal, (b) FFT spectrum of the V(y) signal and (c) FFT spectrum of the V(z) signal.

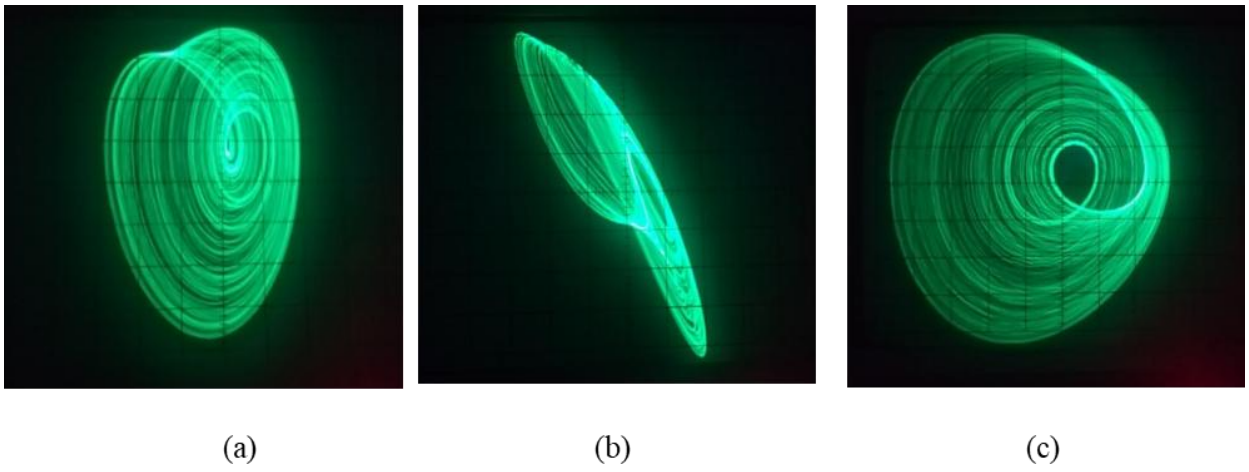

Figure 7. Oscilloscope views: (a) v_x (0.5V/div) versus v_y (0.5V/div), (b) v_x (0.5V/div) versus v_z (0.2V/div), and (c) v_y (0.5V/div) versus v_z (0.2V/div).

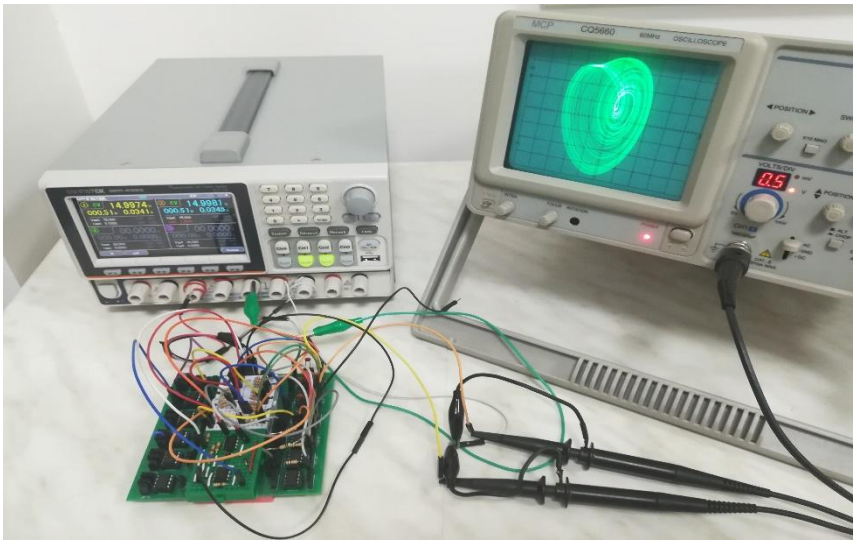

Figure 8. Experimental setup of the novel jerk system with standard components.

5. RBFNN implementations

In this section, we utilize the RBFNN for the validation and analysis of the proposed chaotic jerk system. RBFNN is the type of neural network that consists of mostly three layers: The first one is an input layer, the second one is a hidden layer, and the last is an output layer, as depicted in Figure 9. It is usually used for function approximation, image recognition, time series prediction, and for control systems. First, we model the proposed system using RBFNN and then train the model using the simulated data obtained from the differential equations of the chaotic jerk system in MATLAB. The general formula for the RBFNN model is given by:

$$y(x) = \sum_{k=1}^{m} w_{ki}\, h_k(t) \qquad i=1, 2, 3,\ldots n \tag{8}$$

In the above equation, *w* is the weight of the neural network and y represents the output of the RBFNN. In the first layer of the neural network, a simple transfer function is used as an activation function to transfer the data from the input layer to the hidden layer, but in the case of the hidden layer, there is a nonlinear function used as an activation function for the response of neurons.

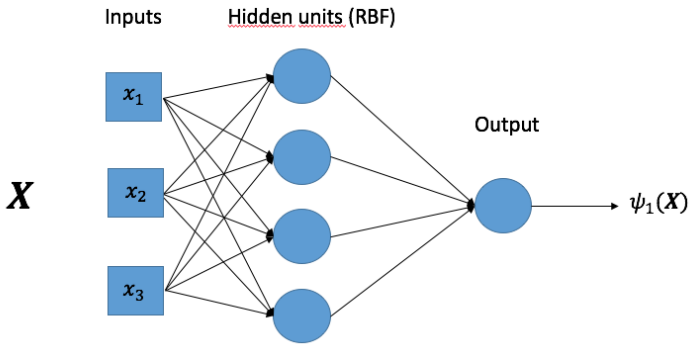

Figure 9. Architecture of RBF network.

In this study, a radial basis function (Gaussian function) is adopted to compute the responses of neurons in the hidden layer of the network. The architecture of the proposed RBFNN model for the chaotic Jerk system is visually represented in Figure 10.

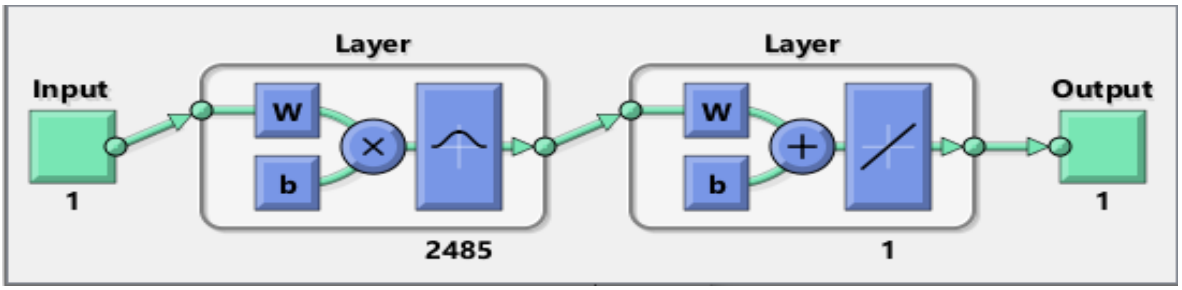

Figure 10. RBFNN architecture of a chaotic Jerk system.

In this research, we introduce a time-varying parametric framework for modeling the behavior and dynamics of the jerk system (1). The approach leverages a neural network architecture built upon radial basis functions, with the system behavior formulated through a corresponding set of mathematical equations:

$$\begin{aligned} x &= \mathrm{RBFNN(t)} + e_1 \\ y &= \mathrm{RBFNN(t)} + e_2 \\ z &= \mathrm{RBFNN(t)} + e_3 \end{aligned} \tag{9}$$

where the parameters x_1, x_2, and x_3 are derived using RBFNN structured around a single input variable t over a defined time interval. The terms e_1, e_2, and e_3 denote the associated computational errors. We use the Euclidean distance formula to measure how far the input is from the center point in the hidden layer. This is done using the following formula:

$$d = \|x(t) - c_i(t)\| \tag{10}$$

Similarly, the output of the hidden layer is calculated using the following formula:

$$h_{j(t)} = exp\left(\frac{\|x(t) - c_i(t)\|^2}{2a_j{}^2}\right), \qquad j= 1, 2, 3\ldots m \tag{11}$$

where a_j represent the width or spread and m is the total number of neurons in the hidden layer. In Eqs (10) and (11), and c_i denotes the center of the i-th radial basis function in the hidden layer. These centers represent fixed points in the input space, typically determined using a clustering method such as k-means, and are used to compute the Euclidean distance that governs each neuron's activation.

The output is found by adding together the weighted values using the formula below:

$$y_i(t) = \sum_{j=1}^{m} w_{ji}\, h_j(t), \qquad i= 1, 2, 3\ldots \tag{12}$$

The performance of a RBFNN is highly influenced by the selection of appropriate center points and function widths. Even minor adjustments to the width can significantly affect each neuron's output, determining whether its response is sharp or broad. The network determines the optimal weights using the least squares method.

We evaluate the accuracy by seeing how close its predictions are to the actual results. To do this, we use something called relative error, which tells us how big the difference is between the predicted and real values. Here is how it is calculated:

$$N_e = \sqrt{\frac{\sum_{i=1}^{n}[y(t_i) - f(t_i)]^2}{\sum_{i}^{n} y(t_i)^2}} \tag{13}$$

In Eq (13), y denotes the actual value, while f represents the predicted output of the neural network.

5.1 Evaluating model precision

RMSE is a widely recognized metric for assessing the accuracy of prediction models, particularly in fields such as machine learning and statistical modeling. It reflects the average size of the errors between predicted values and actual outcomes, offering a clear measure of how well a model performs. RMSE is determined by taking the square root of the average of the squared differences between observed and predicted values. Because of its ability to effectively capture prediction error, RMSE is often used to evaluate model reliability and guide decision-making. In this study, RMSE is applied to assess the performance of a proposed RBFNN in modeling the novel jerk chaotic system. The RMSE value is calculated using the following formula:

$$\mathrm{RMSE} = \sqrt{\frac{1}{\mathrm{N}}\sum_{\mathrm{i}=1}^{\mathrm{N}}(\mathrm{y_i} - \hat{\mathrm{y}}_\mathrm{i})^2} \tag{14}$$

where N represents the total number of sample data.

5.2. Comprehensive evaluation of experimental results

We develop and train an intelligent computational model using a RBFNN, implemented in MATLAB. Training neural networks can be challenging, particularly for complex and unpredictable systems like the novel chaotic Jerk system. To simplify and improve the training process, we use a single combined time input instead of multiple separate values, which enhance the model's learning ability, as illustrated in Figure 11. Figure 12 demonstrates the effectiveness of the RBFNN in accurately modeling the proposed chaotic Jerk system, closely capturing its dynamic behavior. These results confirm the robustness of our approach, even for intricate systems.

To determine the appropriate number of hidden neurons in the RBFNN, an empirical optimization approach is adopted. We begin with a small number of radial basis units and progressively increase the network size while monitoring performance metrics such as RMSE and relative error. The optimal number of neurons is selected as the minimum value at which the performance metrics stabilize, with the MSE reaching the order of 10^{-10}–10^{-9} and the relative error reaching the order of 10^{-9}–10^{-8}, without further improvement when additional units are added. This data-driven selection avoids overfitting while ensuring sufficient approximation capability for the chaotic Jerk system.

Table 2 presents the structural configuration and training dataset used for the RBFNN model developed to approximate the dynamics of the Jerk system (1). The network employs a single time-based input and three output neurons corresponding to the system states ($x(t)$, $y(t)$, and $z(t)$). A total of 2,485 Gaussian radial basis neurons is used in the hidden layer, with centers determined through k-means clustering and a spread parameter of 0.05 to ensure stable generalization. Training data consisting of 10,001 samples are generated using MATLAB's ODE45 solver over a 0–10 s interval with a time step of 0.001 s, and split into 80% for training and 20% for testing. The network weights are optimized using the least squares method, enabling efficient learning of the complex nonlinear patterns inherent in the chaotic system.

Table 2. RBFNN structural configuration and training dataset for the Jerk system (1).

Item	Description/Value
Input variable	Time index t
Output variables	(x(t), y(t), z(t))
Number of input neurons	1
Number of output neurons	3
Number of hidden neurons	2485
Basis function type	Gaussian (RBF)
Spread/Width parameter (σ)	**0.05**
Center selection method	k-means clustering
Weight optimization	Least squares method
Training data length	10,001 points
Training/Testing split	80% / 20%
Integration method (data generation)	MATLAB ODE45
Time interval	0–10 s
Time step	0.001 s

Table 3 presents the training performance of the RBFNN for the three state variables of the Jerk system, demonstrating exceptionally high prediction accuracy across all outputs. The MSE values lie within the range of 10^{-10} to 10^{-9}, indicating extremely small prediction errors, while the MAE and RMSE also remain very low, on the order of 10^{-6} and 10^{-5}, respectively. The relative error values, ranging from 10^{-9} to 10^{-8}, confirm that the network's predicted trajectories closely match the true system dynamics with negligible deviation. All variables converge after 2,450 training epochs, showing that the RBFNN learns the chaotic patterns efficiently and consistently.

Table 3. Training results of RBFNN for Jerk system (1).

Variables	No of nodes	MSE	MAE	RMSE	Relative error	Epochs
x	2485	1.2×10^{-9}	6.4×10^{-6}	3.4×10^{-5}	8.1×10^{-9}	2450
y	2485	9.5×10^{-10}	5.9×10^{-6}	3.1×10^{-5}	7.6×10^{-9}	2450
z	2485	7.8×10^{-9}	8.7×10^{-6}	8.8×10^{-5}	1.1×10^{-8}	2450

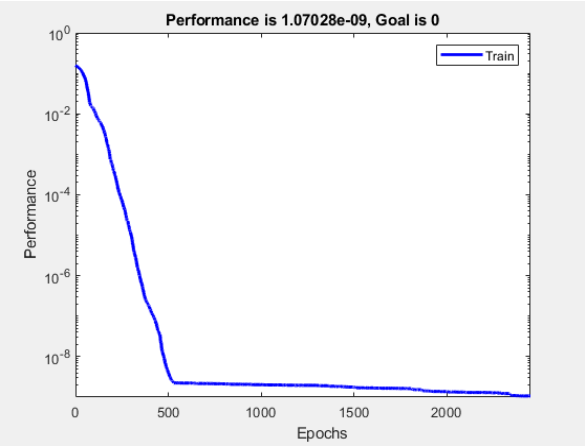

Figure 11. Training performance of RBFNN.

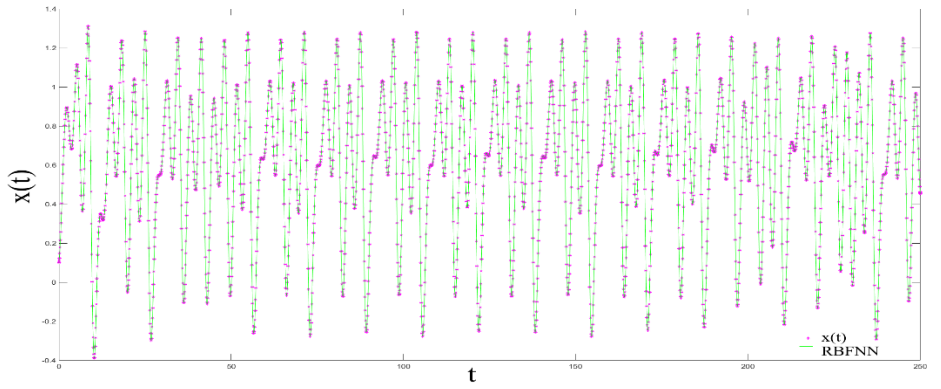

(a)

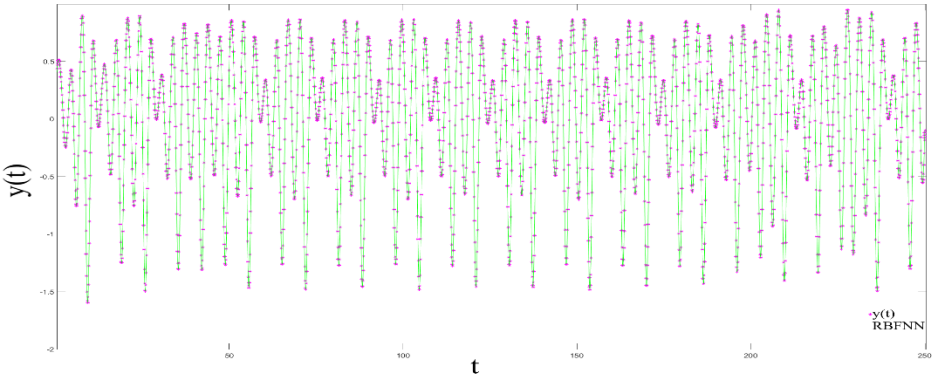

(b)

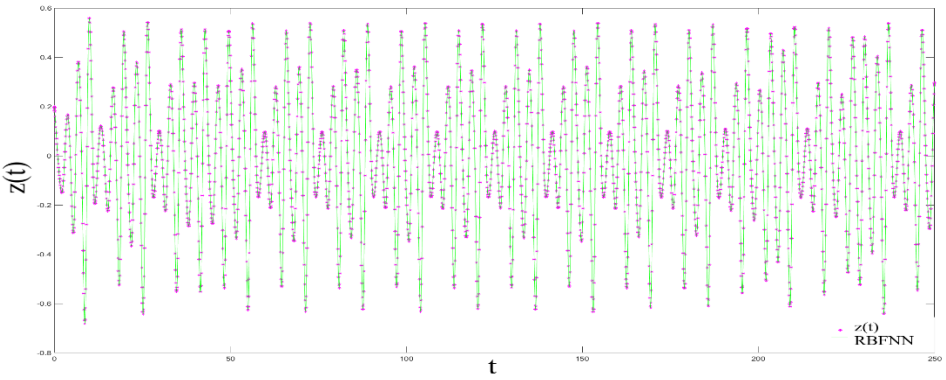

(c)

Figure 12. Parametric comparison for the three signals of Jerk system (1): (a) $x(t)$ signal, (b) $y(t)$ signal, and (c) $z(t)$ signal.

The neural networks learn the system well and reach accurate results after 2,450 training steps. This shows that the model is trained efficiently and can quickly recognize and predict the complex patterns in the chaotic system. The RBFNN model predictions and the exact numerical solutions for the novel chaotic Jerk system are compared in Figure 13. The results show that the model accurately captures the system's chaotic behavior, proving it is a good fit for complex problems like this.

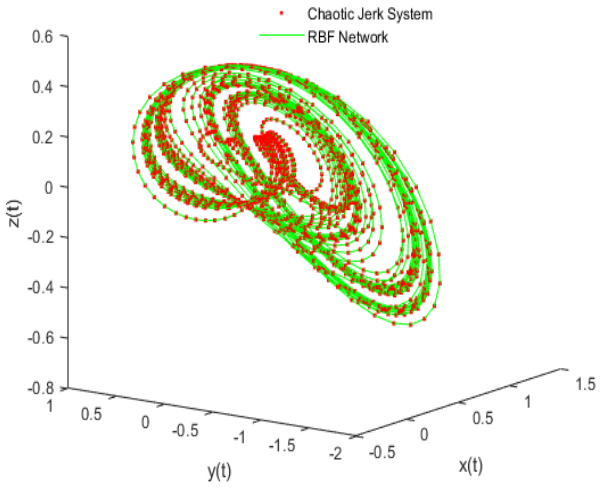

Figure 13. Exact solution and network prediction in Jerk system.

In Figure 13, we show a 3D view of the chaotic Jerk system to compare our RBFNN model with the exact solution. The red dots show the actual calculated values, while the green lines show what the model predicts. This makes it easy to see how closely the model follows the real system.

Similarly, the 2D comparison is presented in Figure 14 for the x, y, and z signals of the chaotic Jerk system, which shows good validation and analysis.

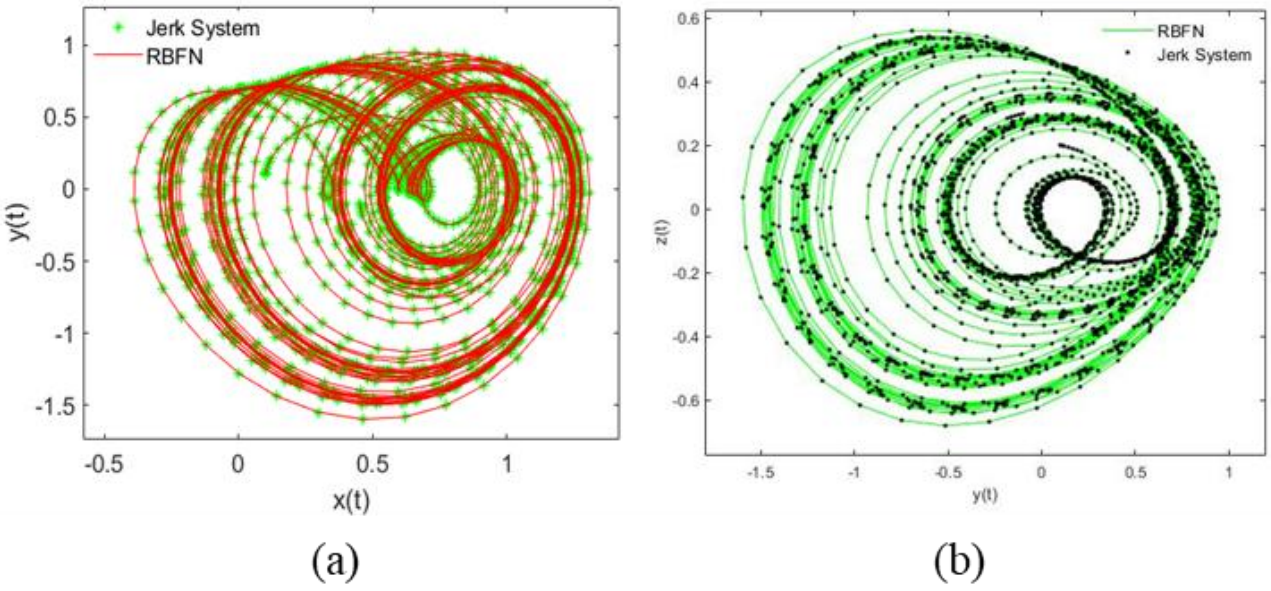

Figure 14. Comparison of exact solution and RBFNN in 2D for chaotic Jerk model: (a) $x(t) - y(t)$ plane and (b) $y(t) - z(t)$.

The error analysis of the RBFNN model for the chaotic Jerk system (1) is presented in Figure 15 across phase spaces. These figures demonstrate the accuracy of the model and confirm the effectiveness of our approach. The error trajectories remain extremely small, with instantaneous error values generally on the order of 10^{-9}, highlighting the reliability and precision of the RBFNN in

capturing the system's dynamics. This exceptional accuracy demonstrates the strong capability of the model to handle the complex and highly sensitive behavior of the chaotic Jerk system.

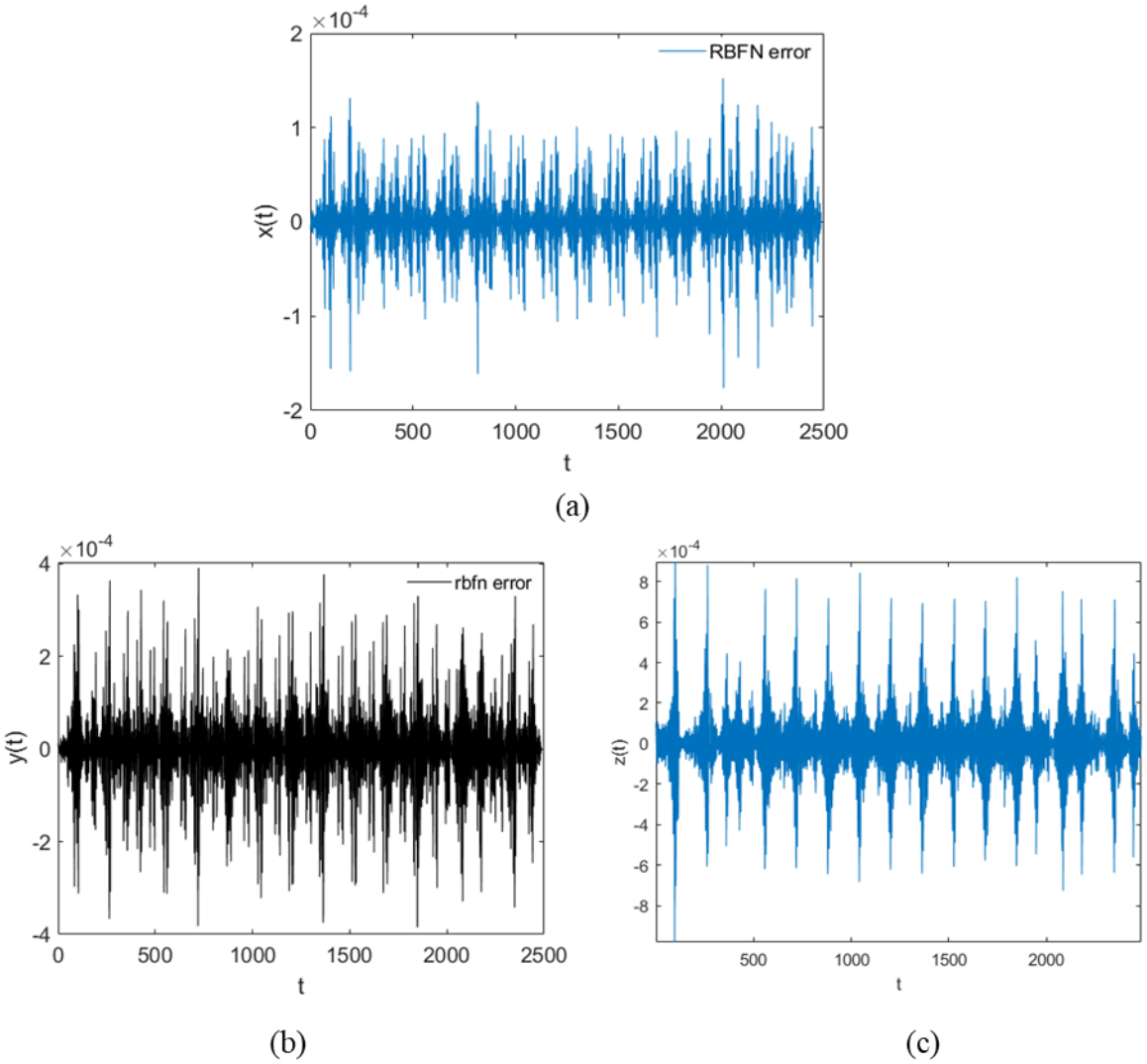

Figure 15. Evaluating RBFNN model errors in different phase spaces: (a) Error signal in the $x(t)$, (b) Error signal in the $y(t)$, and (c) Error signal in the $z\ (t)$.

6. Conclusions

We introduce a chaotic Jerk circuit characterized by symmetrical attractors arising from a combination of sinusoidal, hyperbolic, and absolute nonlinear elements. We explore the system's behavior using well-established numerical methods, including phase portraits, stability analysis, and Lyapunov exponents. Moreover, by adjusting the amplitude, we find that control parameter δ can amplify or attenuate system signals while preserving stability and chaotic properties. To validate our theoretical findings, we perform circuit simulations using Multisim, and the simulated attractors closely match the numerical results. In future work, we will focus on implementing real-time FPGA/CMOS realizations and performing a comprehensive comparison of the RBFNN model with

other advanced machine-learning approaches to further evaluate and improve prediction accuracy.

Author contributions

Aceng Sambas: Conceptualization, Methodology, Formal analysis, Investigation, Writing—original draft preparation; Hatem E. Semary: Conceptualization, Validation, Funding acquisition; Abdullah Gokyildirim: Methodology, Software, Validation, Investigation, Writing—original draft preparation; Sadam Hussain: Validation, Writing—review and editing; Rameshbabu Ramar: Methodology, Software, Investigation, Writing—original draft preparation; Sulaiman M. Ibrahim: Formal analysis, Data curation, Writing—review and editing; A. S. Al-Moisheer: Data curation, Funding acquisition; Rabiu Bashir Yunus: Formal analysis, Data curation, Writing—review and editing. All authors reviewed the results and approved the final version of the manuscript.

Use of Generative-AI tools declaration

The authors declare they have not used Artificial Intelligence (AI) tools in the creation of this article.

Funding statement

This work was supported and funded by the Deanship of Scientific Research at Imam Mohammad Ibn Saud Islamic University (IMSIU) (grant number IMSIU-DDRSP2603).

Conflicts of interest

The authors declare no conflicts of interest to report regarding the present study.

References

1. X. Xu, W. Guo, Chaotic behavior of turbine regulating system for hydropower station under effect of nonlinear turbine characteristics, *Sustain. Energy Technol. Assess.*, **44** (2021), 101088. https://doi.org/10.1016/j.seta.2021.101088
2. M. Ikeda, R. Tada, Reconstruction of the chaotic behavior of the Solar System from geologic records, *Earth Planet. Sci. Lett.*, **537** (2020), 116168. https://doi.org/10.1016/j.epsl.2020.116168
3. A. Sambas, W. S. M. Sanjaya, M. Mamat, O. Tacha, Design and numerical simulation of unidirectional chaotic synchronization and its application in secure communication system, *J. Eng. Sci. Tech. Rev.,* **6** (2013), 66–73.
4. A. Sambas, S. Vaidyanathan, M. Mamat, M. A. Mohamed, W. S. M. Sanajaya, A new chaotic system with a pear-shaped equilibrium and its circuit simulation, *Int. J. Electr. Comput. Eng.*, **8** (2018), 4951. http://doi.org/10.11591/ijece.v8i6.pp4951-4958
5. X. Deng, S. Ding, H. Lin, L. Jiang, H. Sun, J. Jin, Privacy-preserving online medical image exchange via hyperchaotic memristive neural networks and DNA encoding, *Neurocomputing*, **653** (2025), 131132. https://doi.org/10.1016/j.neucom.2025.131132

6. Z. Wang, A. Ahmadi, H. Tian, S. Jafari, G. Chen, Lower-dimensional simple chaotic systems with spectacular features, *Chaos Solitons Fract.*, **169** (2023), 113299. https://doi.org/10.1016/j.chaos.2023.113299
7. Y. Wei, X. Wang, T. Zhao, B. Du, Symmetric coexistence, complete control, circuit implementation, and synchronization of a memristor-coupled jerk chaotic system, *AEU-Int. J. Electron. Commun.*, **197** (2025), 155820. https://doi.org/10.1016/j.aeue.2025.155820
8. P. Li, T. Zheng, C. Li, X. Wang, W. Hu, A unique jerk system with hidden chaotic oscillation, *Nonlinear Dyn.*, **86** (2016), 197–203. https://doi.org/10.1007/s11071-016-2882-2
9. Z. Kohl, R. Senani, D. Biolek, Chaos generation via inductorless jerk circuit: the engineering approach to circuit design and implementation, *IEEE Circ. Syst. Mag.*, **25** (2025), 56–65. https://doi.org/10.1109/MCAS.2025.3559469
10. A. Ahmadi, S. Sriram, A. M. Ali, K. Rajagopal, N. Pal, S. Jafari, A nonlinear megastable system with diamond-shaped oscillators, *Int. J. Bifurcat. Chaos*, **34** (2024), 2450053. https://doi.org/10.1142/S0218127424500536
11. B. Srisuchinwong, R. Treetanakorn, Current-tunable chaotic jerk circuit based on only one unity-gain amplifier, *Electron. Lett*., **50** (2014), 1815–1817. https://doi.org/10.1049/el.2014.3079
12. J. Kengne, R. L. T. Mogue, T. F. Fozin, A. N. K. Telem, Effects of symmetric and asymmetric nonlinearity on the dynamics of a novel chaotic jerk circuit: Coexisting multiple attractors, period doubling reversals, crisis, and offset boosting, *Chaos Solitons Fract.*, **121** (2019), 63–84. https://doi.org/10.1016/j.chaos.2019.01.033
13. R. Chiu, D. López-Mancilla, C. E. Castañeda, O. Orozco-López, E. Villafaña-Rauda, R. Sevilla-Escoboza, Design and implementation of a jerk circuit using a hybrid analog–digital system, *Chaos, Soliton. Fract.*, **119** (2019), 255–262. https://doi.org/10.1016/j.chaos. 2018.12.029
14. P. Chansangiam, Three-saddle-foci chaotic behavior of a modified jerk circuit with Chua's diode, *Symmetry*, **12** (2020), 1803. https://doi.org/10.3390/sym12111803
15. P. Ding, X. Feng, Generation of multi-scroll chaotic attractors from a jerk circuit with a special form of a sine function, *Electronics*, **9** (2020), 842. https://doi.org/10.3390/electronics 9050842
16. P. Li, T. Zheng, C. Li, X. Wang, W. Hu, A unique jerk system with hidden chaotic oscillation, *Nonlinear Dyn*., **86** (2016), 197–203. https://doi.org/10.1007/s11071-016-2882-2
17. M. Joshi, A. Ranjan, An autonomous simple chaotic jerk system with stable and unstable equilibria using reverse sine hyperbolic functions, *Int. J. Bifurcat. Chaos*, **30** (2020), 2050070. https://doi.org/10.1142/S0218127420500704
18. J. R. Mboupda Pone, V. Kamdoum Tamba, G. H. Kom, A. B. Tiedeu, Period-doubling route to chaos, bistability and antimononicity in a jerk circuit with quintic nonlinearity, *Int. J. Dyn. Control*, **7** (2019), 1–22. https://doi.org/10.1007/s40435-018-0431-1
19. C. Ainamon, S. T. Kingni, V. K. Tamba, J. B. C. Orou, P. Woafo, Dynamics, circuitry implementation and control of an autonomous Helmholtz jerk oscillator, *J. Control Autom. Electr. Syst.*, **30** (2019), 501–511. https://doi.org/10.1007/s40313-019-00463-0
20. I. Ahmad, B. Srisuchinwong, Simple chaotic jerk flows with families of self-excited and hidden attractors: Free control of amplitude, frequency, and polarity, *IEEE Access*, **8** (2020), 46459–46471. https://doi.org/10.1109/ACCESS.2020.2978660
21. A. Sambas, X. Zhang, I. A. Moghrabi, S. Vaidyanathan, K. Benkouider, M. Alçın, et al., ANN-based chaotic PRNG in the novel jerk chaotic system and its application for the image encryption via 2-D Hilbert curve, *Sci. Rep.*, **14** (2024), 29602. https://doi.org/10.1038/s41598-024-80969-z

22. M. H. Arshad, M. Kassas, A. E. Hussein, M. A. Abido, A simple technique for studying chaos using jerk equation with discrete time sine map, *Appl. Sci.*, **11** (2021), 437. https://doi.org/10.3390/app11010437
23. Q. Xu, S. Cheng, Z. Ju, M. Chen, H. Wu, Asymmetric coexisting bifurcations and multi-stability in an asymmetric memristive diode-bridge-based jerk circuit, *Chin. J. Phys.*, **70** (2021), 69–81. https://doi.org/10.1016/j.cjph.2020.11.007
24. S. Sahoo, R. Nathasarma, B. K. Roy, Time-synchronized predefined-time synchronization between two non-identical chaotic systems, *Chaos Solitons Fract.*, **181** (2024), 114662. https://doi.org/10.1016/j.chaos.2024.114662
25. C. Zhang, B. Zhang, J. Chen, A. Pan, Z. Tan, Y. Yao, et al., Controllable multi-scroll with multi-wing, grid-scroll, and multi-directional grid-scroll chaotic attractors in a chaotic system with implicit Duffing equation, *Eur. Phys. J. Plus*, **139** (2024), 492. https://doi.org/10.1140/epjp/s13360-024-05295-9
26. A. Gokyildirim, H. Calgan, M. Demirtas, Fractional-order sliding mode control of a 4D memristive chaotic system, *J. Vib. Control*, **30** (2024), 1604–1620. https://doi.org/10.1177/10775463231166
27. H. Liu, W. Niu, Y. Guo, Direct torque control for PMSM based on the RBFNN surrogate model of electromagnetic torque and stator flux linkage, *Control Eng. Pract.*, **148** (2024), 105943. https://doi.org/10.1016/j.conengprac.2024.105943
28. F. A. Jibon, A. Tasbir, M. A. Talukder, M. A. Uddin, F. Rabbi, M. S. Uddin, et al., Parkinson's disease detection from EEG signal employing autoencoder and RBFNN-based hybrid deep learning framework utilizing power spectral density, *Digit. Health*, **10** (2024), 7355. https://doi.org/10.1177/20552076241297355
29. P. M. Kumar, R. Dhilipkumar, G. Geethamahalakshmi, Efficient distribution network based on photovoltaic fed electric vehicle charging station using WSO-RBFNN approach, *J. Energy Storage*, **106** (2025), 114728. https://doi.org/10.1016/j.est.2024.114728
30. A. Z. Messaoui, O. Mechali, A. A. Messaoui, I. E. Smaali, F. Demim, D. B. Djilali, RBFNN-based optimized PID control for a 3-DOF helicopter system: Design and validation, *2024 8th International Conference on Image and Signal Processing and their Applications*, 2024, 1–5. https://doi.org/10.1109/ISPA59904.2024.10536810
31. Y. Li, W. Sun, D. Yu, RBFNN-based global fast terminal sliding mode control for fully controlled doubly fed induction generator, *J. Franklin Inst.*, **361** (2024), 107196. https://doi.org/10.1016/j.jfranklin.2024.107196
32. T. Yuan, C. Zhang, F. Yi, P. Lv, M. Zhang, S. Li, RBFNN-based adaptive integral sliding mode feedback and feedforward control for a lower limb exoskeleton robot, *Electronics*, **13** (2024), 1043. https://doi.org/10.3390/electronics13061043
33. Z. Zhang, E. Zhu, B. Wang, Y. Chen, Application and comparison of GRNN, BPNN and RBFNN in the prediction of suspender frequency and tension on arch bridge, *J. Civ. Struct. Health Monit.*, **14** (2024), 1839–1855. https://doi.org/10.1007/s13349-024-00816-7
34. M. Lu, W. Yang, Z. Xiong, F. Liao, S. Wu, Y. Su, et al., RBFNN-based adaptive fixed-time sliding mode tracking control for coaxial hybrid aerial–underwater vehicles under multivariant ocean disturbances, *Drones*, **8** (2024), 745. https://doi.org/10.3390/drones8120745

35. A. Nanfak, J. de Dieu Nkapkop, K. Zourmba, J. M. Ngono, M. F. Moreno-López, E. Tlelo-Cuautle, et al., Dynamic analysis and FPGA implementation of a 2D fractional sine-cosine map for image encryption using bit-level permutation and genetic algorithm, *Math. Comput. Simul.*, **240** (2026), 105–136. https://doi.org/10.1016/j.matcom.2025.07.022
36. J. Zhang, N. Cheng, P. Wang, Dynamics analysis, FPGA implementation, and application in image encryption of a quadruple-wing chaotic system based on hyperbolic sine functions, *Integration*, **104** (2025), 102437. https://doi.org/10.1016/j.vlsi.2025.102437
37. E. Juárez-Mendoza, G. Zamora-Mejia, E. Tlelo-Cuautle, A. Díaz-Sánchez, CMOS design of a chaos-based masking system for biomedical signals applications, *Int. J. Circuit Theory Appl.*, **53** (2025), 5802–5815. https://doi.org/10.1002/cta.4500
38. Z. Duan, X. Zhang, S. He, X. Yu, P. Xiong, J. Chen, et al., Implementation of a fully integrated memristive Chua's chaotic circuit with a voltage-controlled oscillator, *Integration*, **99** (2024), 102258. https://doi.org/10.1016/j.vlsi.2024.102258
39. C. K. Volos, L. Moysis, G. D. Roumelas, A. Giakoumis, H. E. Nistazakis, G. S. Tombras, Circuit implementation of a modified chaotic system with hyperbolic sine nonlinearities using bi-color LED, *Technologies*, **9** (2021), 15. https://doi.org/10.3390/technologies9010015
40. J. Kengne, L. K. Kengne, J. C. Chedjou, K. Nosirov, A simple anti-parallel diode based chaotic jerk circuit with arcsinh function: Theoretical analysis and experimental verification, *Analog Integr. Circuits Signal Process.*, **108** (2021), 597–623. https://doi.org/10.1007/s10470-021-01876-1

AIMS Press